AGU PUBLICATIONS

Water Resources Research

RESEARCH ARTICLE
10.1002/2014WR015815

Modification of the Local Cubic Law of fracture flow for weak inertia, tortuosity, and roughness

Lichun Wang[1], M. Bayani Cardenas[1], Donald T. Slottke[2], Richard A. Ketcham[1], and John M. Sharp Jr.[1]

[1]Department of Geological Sciences, University of Texas at Austin, Austin, Texas, USA, [2]Schlumberger, Houston, Texas, USA

Key Points:
- We present a modified Local Cubic Law for hydraulic properties of fractures
- The MLCL takes into account tortuosity, roughness, and weak inertial effects
- The MLCL improves estimating effective and local volumetric flow rate

Supporting Information:
- Supporting Information S1
- Data Set S1
- Data Set S2

Correspondence to:
L. Wang,
wanglichun@utexas.edu

Citation:
Wang, L., M. B. Cardenas, D. T. Slottke, R. A. Ketcham, and J. M. Sharp (2015), Modification of the Local Cubic Law of fracture flow for weak inertia, tortuosity, and roughness, *Water Resour. Res.*, *51*, doi:10.1002/2014WR015815.

Received 7 MAY 2014
Accepted 1 MAR 2015
Accepted article online 6 MAR 2015

Abstract The classical Local Cubic Law (LCL) generally overestimates flow through real fractures. We thus developed and tested a modified LCL (MLCL) which takes into account local tortuosity and roughness, and works across a low range of local Reynolds Numbers. The MLCL is based on (1) modifying the aperture field by orienting it with the flow direction and (2) correcting for local roughness changes associated with local flow expansion/contraction. In order to test the MLCL, we compared it with direct numerical simulations with the Navier-Stokes equations using real and synthetic three-dimensional rough-walled fractures, previous corrected forms of the LCL, and experimental flow tests. The MLCL performed well and the effective errors (δ) in volumetric flow rate range from -3.4% to 13.4% with an arithmetic mean of $|\delta|$ ($<|\delta|>$) equal to 3.7%. The MLCL is more accurate than previous modifications of the LCL. We also investigated the error associated with applying the Cubic Law (CL) while utilizing modified aperture field. The δ from the CL ranges from -14.2% to 11.2%, with a slightly higher $<|\delta|> = 6.1\%$ than the MLCL. The CL with the modified aperture field considering local tortuosity and roughness may also be sufficient for predicting the hydraulic properties of rough fractures.

1. Introduction

The fundamental understanding of fluid flow and transport processes through connected fractures is critical for many environmental and engineering problems and geophysical phenomena. However, detailed characterization of flow and transport processes within complex fracture networks remains a challenge, thus numerous studies have been focused on discrete single rough-walled fractures [e.g., *Zimmerman et al.*, 2004; *Cardenas et al.*, 2007].

Incompressible, steady state fluid flow through single fractures is governed by the Navier-Stokes equations (NSE) and the mass conservation equation:

$$\rho(\mathbf{u}\cdot\nabla)\mathbf{u} = -\nabla p + \mu\nabla^2\mathbf{u} \tag{1}$$

$$\nabla\cdot\mathbf{u} = 0 \tag{2}$$

where ρ is fluid density, $\mathbf{u} = [u, v, w]$ is velocity vector, p is total pressure, and μ is dynamic fluid viscosity. Even though the direct solution of the NSE is theoretically the most accurate approach for analyzing the hydraulic properties of fractures, solving the NSE through three-dimensional (3-D) rough-walled fractures is a substantial computational endeavor with only a few studies having successfully implemented this [*Zimmerman et al.*, 1991; *Sisavath et al.*, 2003].

To circumvent the difficulty in solving the NSE, the nonlinear/inertial terms in the NSE are often neglected. Vertical integration of the resulting simplified NSE, now called the Stokes equation, results in the well-known Cubic Law (CL) [e.g., *Snow*, 1969; *Witherspoon et al.*, 1980] that shows the volumetric flow rate through a fracture is a linear function of the head gradient and the cube of the hydraulic aperture, with the latter representing the transmissivity of the fracture. However, the surface roughness of fractures has a significant influence on fluid flow, which leads to deviation of the flow rate predicted by the CL from the actual flow rate [e.g., *Brown*, 1987; *Zimmerman et al.*, 1992]. The CL's accuracy can be improved by incorporating a correction factor based on fracture roughness [*Renshaw*, 1995]. Another approach is to consider explicitly the spatial variability in aperture field that results in what is known as the classical Local Cubic Law (LCL) [*Zimmerman et al.*, 1991; *Mourzenko et al.*, 1995; *Nicholl et al.*, 1999].

The classical LCL, sometimes called the Reynolds equation, has been extensively applied in investigations of fluid flow, and related conservative and reactive solute transport through a single fracture [e.g., *Zimmerman et al*., 1991; *Nicholl et al*., 1999; *Elkhoury et al*., 2013]. It reads as:

$$\nabla \cdot \left(b^3 \nabla p\right) = 0 \tag{3}$$

where b is the apparent (or vertical) local aperture, which is the difference in height between the top and bottom fracture surfaces, and b^3 constitutes the local fracture transmissivity.

One of the limitations of the classical LCL is the assumption that the fracture midsurface is a flat plane, whereas natural fractures characteristically exhibit a tortuous plane [*Ge*, 1997]. Additionally, local velocity profiles in real fractures deviate from the assumed parabolic shape, i.e., Poiseuille flow, due to roughness and inertial effects. Therefore, there are outstanding questions regarding the broad applicability of the LCL. Numerous efforts have attempted to quantify criteria wherein the LCL can be used in lieu of the NSE, but the results have been mixed. For example, *Brush and Thomson* [2003] defined geometric and kinematic constraints that ensure the validity of the LCL. *Brown et al*. [1995] earlier suggested the same constraint, $Re < 1$, accounting for inertial force, where Re is the Reynolds Number. On the contrary, *Konzuk and Kueper* [2004] found that even at $Re < 1$, the LCL could overestimate flow rate by at least 1.75 times. Another study showed that the LCL overestimated flow rates by 22–47% [*Nicholl et al*., 1999]. The discrepancy boils down to the assumptions underlying the traditional LCL, i.e., neglection of either tortuosity, roughness, or inertial force in previous studies.

Ideally, the effective hydraulic properties of fractures could be calculated exclusively from geometric information, and therefore flows can in turn be predicted simply with the additional knowledge of head gradients. Achieving this first requires a more comprehensive representation of local processes that will be used for upscaling. Thus, to improve the accuracy of the LCL, *Ge* [1997] derived a governing equation of the LCL for characterizing fluid flow through 3-D rough-walled fractures that uses a local coordinate system to allow for local tortuosity. However, the verification of the governing equation was done only for two-dimensional (2-D) nonparallel and parallel sinusoidal fractures. *Brush and Thomson* [2003] and *Mallikamas and Rajaram* [2010] applied the LCL while accounting for local roughness and/or tortuosity in 3-D systems, but their results were verified using the Stokes equations, and not the full NSE with inertial effects.

Accurate estimation of flow process through rough and tortuous fractures aids in understanding transport problems in fractured media, and can provide a method to estimate effective transport parameters based on the geometric properties of fractures [*Wang and Cardenas*, 2014]. For example, *Detwiler et al*. [2000] found through their experiments that a velocity field generated from solving the LCL underestimates the longitudinal dispersion coefficient by 20–37% when the Peclet Number increases from 0 to ~800. To compensate for the discrepancy in flow rate from using the LCL, *Detwiler et al*. [2002] introduced a coefficient based on experimental flow information. However, without prior knowledge from flow experiments, the potential application of this correction for the LCL in simulating transport process is not clear.

We present the modified LCL (MLCL) in this study with the goal of developing a robust and accurate but easy to implement method for predicting fracture hydraulic properties and flow rates. Our approach combines ideas from *Ge* [1997], for correcting for local tortuosity, from *Renshaw* [1995], for correcting for local roughness, and additionally considers low inertial effects where local $Re \leq 1$. To assess the performance of the MLCL, effective and local flow rates based on the MLCL are compared to those from direct numerical simulations with the NSE, previous modified versions of the LCL, and experimental flow tests for 3-D rough-walled fractures.

2. Development of Modified Local Cubic Law

2.1. Consideration for Tortuosity

Tortuosity is a macroscopic feature defined as the ratio of actual flow path length over a straight-line distance. Normally, the actual flow field can be obtained through either direct simulation or experimental observation, and it varies depending on aperture field and Re. Thus, it is difficult to correct the LCL with macroscopic tortuosity since this rests on precise knowledge of flow paths. To avoid this situation, here we consider the geometric tortuosity (hereafter, we simply use tortuosity, τ) as the factor defining or a

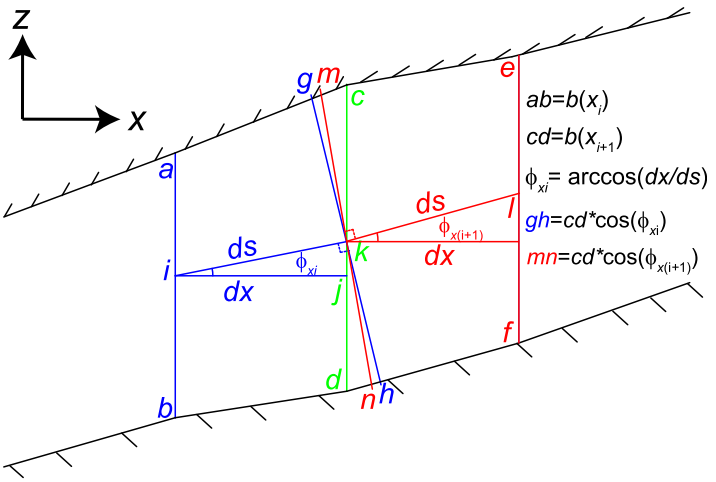

Figure 1. Definition of flow-oriented apertures (blue line *gh* and red line *mn*) modified from *cd* in the *x* direction accounting for tortuosity of two contiguous flow cells. *ab*, *cd*, and *ef* are apparent apertures $b(x_i)$, $b(x_{i+1})$, and $b(x_{i+2})$, respectively, *i*, *k*, and *l* are the central aperture points. *ik* represents the actual length of a flow path (*ds*), *ij* is the straight-line distance (*dx*) between the ends of the flow path. Tortuosity is defined as *ds*/*dx* with calculated orientation angle ϕ_{xi}. Calculation of flow-oriented aperture follows the above equations.

surrogate for a tortuous flow path. τ is defined as the ratio of the actual 3-D tortuous midsurface plane to the projected area in the *x*-*y* 2-D plane; this follows the work of *Ge* [1997], and it represents the increased flow path length due to variation of the midsurface plane of the aperture field. To determine local tortuosity, we define *ds* as the actual length of a flow path and *dx* as the straight-line distance between the ends of the flow path as illustrated in Figure 1. Thus by definition, local tortuosity is the ratio of *ds* to *dx*. Since the tortuosity varies over space, any given interior apparent aperture could be thus translated into a pair of flow-oriented apertures for two contiguous flow cells. For example, the flow-oriented aperture field b_f in the *x* direction (and also similarly in the *y* direction) for the left or upstream flow cell is approximated by:

$$b_f(x) = b(x_i)\cos(\varnothing_{xi}) \tag{4}$$

where $b(x_i)$ is the apparent aperture and ϕ_{xi} is the flow orientation angle estimated from the definition of tortuosity for the left flow cell (Figure 1). Moreover, since tortuosity varies with direction, the apparent aperture field can be transformed into an anisotropic flow-oriented aperture field b_f, with independent *x* and *y* components in the principal directions. Components in other directions are eliminated that is also a fundamental assumption behind the LCL.

The transmissivity vector (*T*) between cells can be estimated using a harmonic mean of adjacent flow-oriented apertures in the *x* and *y* directions, which has been tested to be the most accurate approximation at local scale [e.g., *Nicholl et al*., 1999; *Nicholl and Detwiler*, 2001]. For example, the component of *T* in the *x* direction (T_x) can be approximated by:

$$T_x = \frac{2b_f(x_{i+1})^3 b_f(x_i)^3}{b_f(x_{i+1})^3 + b_f(x_i)^3} \cdot \frac{1}{12\mu} \tag{5}$$

Replacing b^3 in equation (3) with *T* (equation (5)) and accounting for the tortuosity translates the LCL from the local coordinate (i.e., the actual flow path direction $\boldsymbol{s}$) to the global coordinate (i.e., the *x* and *y* directions):

$$\nabla \cdot \left[T_x \frac{\partial p}{\partial x}\frac{\partial x}{\partial \boldsymbol{s}} \vec{i} + T_y \frac{\partial p}{\partial y}\frac{\partial y}{\partial \boldsymbol{s}} \vec{j} \right] = \nabla \cdot \left[T_x \frac{\partial p}{\partial x}\cos(\varnothing_x)\vec{i} + T_y \frac{\partial p}{\partial y}\cos(\varnothing_y)\vec{j} \right] = 0 \tag{6}$$

where $\vec{i}$ and $\vec{j}$ represent the unit vectors in *x* and *y* directions, respectively.

2.2. Rationale for Consideration for Local Roughness and Weak Inertial Effects

Many experimental and numerical studies have illustrated the effects of roughness and inertia on flow through fractures [e.g., *Brown*, 1987; *Thompson and Brown*, 1991]. For example, nonparabolic velocity profile developed in a sinusoidal fracture can result in the overestimation of flow rate predicted by the LCL [*Brush and Thomson*, 2003]. The formation of an eddy in rough fractures represents the extreme case of a nonparabolic velocity profile. Recent researches have shown eddies can form and grow thereby reducing the

Table 1. Input Parameters for Synthetic Fracture Generation Using the Program SynFrac [*Ogilvie et al.*, 2006], and Statistical Properties of Both Real Fractures Mapped Through High-Resolution X-ray Computed Tomography and Synthetic Fractures[a]

	HRXCT			Synthetic				
Parameters	H1	H2	H3	S1	S2	S3	S4	H2R
Length (mm)	116.1	97.9	80.3	95.9	96.8	100.0	100.0	97.9
Width (mm)	140.0	121.8	94.8	95.9	96.8	100.0	100.0	121.8
Resolution (mm^2)	0.077	0.068	0.038	0.035	0.036	0.038	0.038	0.068
Mismatch wavelength (mm)				4.5	2.5	2.3	8.0	
Transition length (mm)				40.0	90.0	72.0	31.0	
Maximum matching fraction				0.98	0.99	0.99	0.99	
Minimum matching fraction				−0.02	−0.06	0.00	−0.09	
Fractal dimension				2.64	2.69	2.78	2.67	
Anisotropy				1.02	1.07	0.76	1.01	
σ_b (mm)	0.59	0.60	0.86	0.36	0.21	0.35	0.31	1.18
$<b>$ (mm)	1.50	1.91	2.14	1.61	1.02	1.53	1.70	4.22
τ	1.033	1.038	1.164	1.062	1.099	1.080	1.080	1.038
$R1$	−11.1 to 12.3	−16.6 to 20.2	−16.9 to 17.2	−5.3 to 5.9	−3.9 to 4.1	−3.8 to 3.7	−3.8 to 3.7	−34.4 to 30.3
$<\|R1\|>$	0.34	0.25	0.56	0.90	0.67	0.64	0.58	1.64
$R2$	0.03–4.31	0.04–0.55	0.02–114	0.06–5.13	0.10–2.68	0.068–1.47	0.11–1.86	0.025–0.38
$<R2>$	0.22	0.08	0.14	0.15	0.23	0.14	0.23	0.07
$Re = \rho<u>/\mu$	0.02	0.02	0.05	0.02	0.01	0.01	0.03	0.06

[a]The mismatch wavelength, transition length, maximum matching fraction, minimum matching fraction, fractal dimension, and anisotropy are the input parameters for SynFrac. Details of the fracture generation using the parameters below can be found at *Ogilvie et al.* [2006]. b represents the apparent aperture with arithmetic mean $<b>$ and standard deviation σ_b. τ refers to the effective tortuosity, defined as the ratio of the tortuous area of the fracture midsurface to its projected area in the x-y plane. $R1$ and $R2$ indicate the local roughness as defined in equations (7) and (8), $<|R1|>$ and $<|R2|>$ represent the arithmetic mean values of $R1$ and $R2$, respectively. The Reynolds Number (Re) is defined as the ratio of inertial force to viscous force, where ρ is a fluid density and μ is a dynamic fluid viscosity.

hydraulic conductivity of fractures and pores [*Cardenas et al.*, 2007; *Chaudhary et al.*, 2011, 2013; *Lee et al.*, 2014]. Moreover, eddy geometry is dependent on flow direction and inertial force [*Chaudhary et al.*, 2011].

In this study, we take into account local roughness and low Re to further improve equation (6). Since aperture variability and local aspect ratio are key local roughness factors that reduce the accuracy of simple harmonic averaging for calculation of flow rates [*Basha and El-Asmar*, 2003], we focus on these two factors. To distinguish the bulk roughness, a global or macroscale feature as referred to by *Brush and Thomson* [2003], from local roughness in this study; hereafter, we refer only to local roughness and associated local aperture gradient and aspect ratio, unless otherwise stated.

The first factor of local roughness is aperture gradient ($R1$) that describes local fracture expansion or contraction relative to one with parallel walls. Expansions or contractions are effectively what constitutes local roughness as a fracture without expansions/contractions is basically represented by parallel plates, i.e., where flow follows Poiseuille flow with perfect parabolic velocity profile that is the basis for the classical LCL. In this study, $R1$ is defined as:

$$R1 = \frac{b_f(x_{i+1}) - b_f(x_i)}{dx} \tag{7}$$

where the calculations of flow-oriented apertures $b_f(x_i)$, and $b_f(x_{i+1})$ are illustrated in Figure 1. $R1$ can be positive or negative depending on whether the fracture expands or contracts relative to the flow direction. The range and arithmetic mean value of $R1$ on both x and y directions are listed in Table 1. The $R1$ field may be anisotropic with independent x and y components since the b_f field is also anisotropic in the principal directions. The resolution of $R1$ depends on the fracture resolution as shown in Table 1.

The second factor of local roughness, the dimensionless length ($R2$), represents the aspect ratio of the fracture. The definition of $R2$ is:

$$R2 = \frac{dx}{b_f(x_i)} \tag{8}$$

where dx is the horizontal resolution of the aperture field and $b_f(x_i)$ is the upstream flow-oriented aperture for each flow cell (Figure 1). $R2$ may also be anisotropic like $R1$, with independent components in the x and y directions.

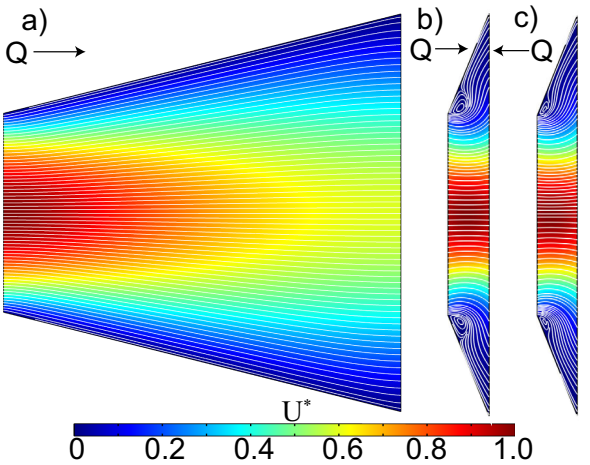

Figure 2. Normalized velocity (U*) field and streamlines (white lines) of 2-D wedges with different local aperture gradient *R*1 and local Reynolds Number *Re*. U* is defined as $U^* = U/U_{max}$, where U is the velocity magnitude and U_{max} is the maximum velocity magnitude. Black arrows indicate flow direction with flow rates Q. Expanding fracture (a) corresponds to $R1 = 0.5$ and $Re = 1.2$ with streamlines showing nonparabolic velocity profile but no eddy growth; expanding fracture (b) corresponds to $R1 = 5$ and $Re = 1.02$, where streamlines indicate eddy growth; contracting fracture (c) corresponds to $R1 = -5$ and $Re = 1.2$, with streamlines showing different eddy geometry compared to fracture in Figure 2b even though they have identical magnitudes of *R*1 and *Re*.

The tortuosity correction can effectively transform the local asymmetric aperture field into piecewise symmetric wedges, where fluid is assumed to flow along the wedge centerline. Thus, to further quantify the associated errors with local roughness resulting in nonparabolic velocity profile, we first conducted CFD simulations of a suite of symmetric 2-D wedges representing a wide range of *R*1 (−50–50) and *R*2 (0–10). This was achieved by running simulations where b_f at one end was fixed, but b_f at the other end and *dx* were sequentially increased (Figures 1 and 2) to produce wedges with different *R*1 and *R*2. For each wedge, simulations were conducted for both flow directions driven by a pressure gradient. These two cases have very opposite *R*1. Furthermore, we increased the pressure gradient successively to consider the effect of low inertial force, i.e., varying Reynolds Number ($Re \leq 1$).

The local *Re* quantifies the ratio of inertial force to viscous force, which is defined as:

$$Re = \frac{\rho b_f \langle u \rangle}{\mu} = \frac{\rho Q}{\mu} \tag{9}$$

where $<u>$ is the local mean velocity and *Q* is the volumetric flow rate per unit fracture width. In this study, we only considered local $Re \leq 1$ to ensure local laminar flow. We employed COMSOL Multiphysics to solve the NSE describing flow through the designed wedges. The simulation results were validated by comparing numerical simulation results to analytical solutions provided by *Basha and El-Asmar* [2003]; the maximum error in predicting volumetric flow rate was less than 0.14% (Figure 3). We only used a fraction of the designed wedges in this validation because only a minority of the wedges satisfy the condition for the analytical solution (i.e., the ratio of arithmetic mean aperture to the fracture length should be less than 1).

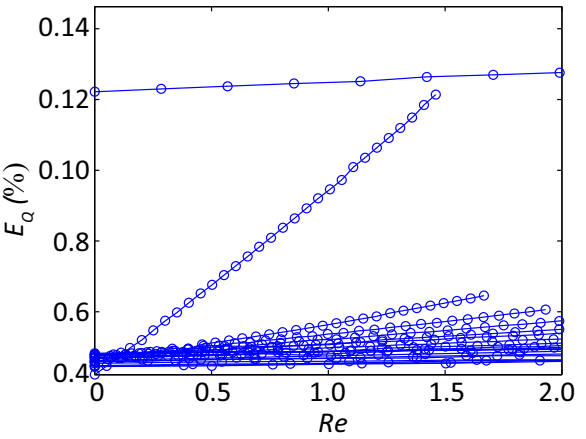

Figure 3. Simulation errors (E_Q) in volumetric flow rate (Q) through symmetric wedges with varying Reynolds Numbers (*Re*). E_Q is defined by $E_Q = (Q_{Bash}/Q_{CFD} - 1) \times 100\%$, where Q_{Bash} was estimated by using the perturbation method proposed by *Basha and El-Asmar* [2003], Q_{CFD} was computed by directly solving the NSE through finite element modeling.

2.3. Correction Coefficient C(R1, R2, Re)

The analytical flow rate Q_{LCL} for 2-D fractures calculated with the LCL is approximated by the harmonic mean of the cubic aperture multiplied by the pressure gradient [*Silliman*, 1989]:

$$Q_{LCL} = \frac{1}{12\mu} \frac{L}{\left(\int_0^L \frac{1}{b_f(x)^3} dx \right)} \frac{\partial p}{\partial x} \tag{10}$$

where $\partial p/\partial x$ is the same pressure gradient as applied in the numerical wedge models. Therefore, for flow rate calculations based on the LCL to match the true flow rates (i.e., from the CFD simulations), it has to be

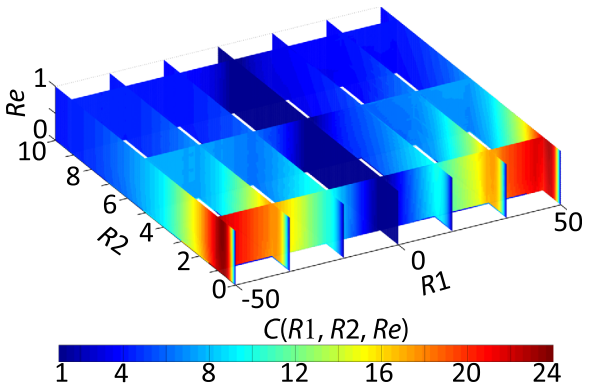

Figure 4. Empirical generic correction factor $C(R1, R2, Re)$ based on CFD simulations, where $R1$ and $R2$ are the local roughness defined in equations (7) and (8), respectively. Re refers to local Reynolds Number.

scaled by the factor C that varies depending on $R1$, $R2$, and Re:

$$C(R1,\ R2,\ Re)=\frac{Q_{\mathrm{LCL}}}{Q_{\mathrm{CFD}}} \tag{11}$$

This can also potentially correct the analytical effective aperture by scaling it to an effective transmissivity which considers fracture expansion or contraction and low inertial effects. The factor C was calculated based on simulations representing various combinations of $R1$, $R2$, and Re (Figure 4). The discrete function C was generated based on adaptive increments; we used a higher resolution where there were larger gradients. Specifically, increments for $|R1|$ ranged from ~0.5, where $0 < |R1| < 3.5$, to ~2.5, where $3.5 < |R1| < 50$. Increments for $R2$ ranged from ~0.01, where $0 < R2 < 1$, to ~2, where $1 < R2 < 10$. Moreover, the increments for Re were almost uniform at ~0.1. The discrete data for C are available on line as supporting information.

The correction factor C fundamentally embodies the effects of local roughness and low inertia which are manifested in the prediction of local velocities and volumetric flow rates (Figure 4). That is, and as expected, $C \geq 1$ since calculations using the LCL with the harmonic mean aperture as the effective transmissivity consistently overestimates the flow rate [e.g., *Brown*, 1987; *Zimmerman et al.*, 1991; *Brown et al.*, 1995]. The LCL is missing additional resistance imparted by local roughness and additional inertial losses. This explanation is also supported by theory [*Basha and El-Asmar*, 2003].

Moreover, for any given $R1$ (but excluding $R1 = 0$), C initially increases with increasing $R2$ ($0 < R2 < 0.5$) but then decreases with further increases in $R2$ ($0.5 < R2 < 10$); note that the dependence of C on $R2$ is also partially determined by $R1$. Since $R1 = 0$ corresponds to parallel plates, we expect no error with increasing $R2$ in this case, i.e., $C = 1$.

The characteristics of C can be explained generally by the formation of nonparabolic velocity profile against that predicted from the LCL, and by the extreme case of growth of eddies within the piecewise wedges of the fracture. Small $R2$ implies a short fracture wavelength or small aspect ratio, which in turn provides insufficient room for the fully developed nonparabolic velocity and for eddy growth. The peak of C is at $R2 \sim 0.5$, regardless of $R1$, which corresponds to the wedge aspect ratio optimal for reducing the effective flow area. These effects of local fracture aspect ratio on predicting flow rate were not considered in previous studies [e.g., *Nicholl et al.*, 1999; *Brush and Thomson*, 2003].

Additionally, $R1$ rather than Re largely determines C when $Re \leq 1$ (Figure 4) for the specific value of $R2$. This is supported by the experimental results of *Lee et al.* [2014], and reflected by the fluid flow following Darcy's law at relatively low Re regime [*Al-Yaarubi et al.*, 2005]. That is, Re contributes little to the deviation from linearity of the flow rate. Moreover, flow direction had a trivial impact on C, and C exhibited a fairly but not perfectly symmetric pattern. This is because fluid flow is different for expanding and contracting fractures [*Cardenas et al.*, 2009; *Chaudhary et al.*, 2011], which lead to different nonparabolic velocity profiles and eddy configuration, even if their $|R1|$ and Re are almost the same (Figure 2).

2.4. Modified Local Cubic Law

Equation (6) can be corrected for effects of local roughness and low inertial force through the application of C, which gives the modified LCL (MLCL):

$$\nabla \cdot \left[\frac{T_x}{C}\frac{\partial p}{\partial x}\cos\left(\varnothing_x\right)\vec{i}+\frac{T_y}{C}\frac{\partial p}{\partial y}\cos\left(\varnothing_y\right)\vec{j}\right]=0 \tag{12}$$

When the midsurface of the aperture field lies in a smooth plane, i.e., where $\vec{\varnothing} = 0$, and when local roughness and inertial force are negligible, $C \sim 1$, the MLCL reduces to the classical LCL. The MLCL is a nonlinear differential equation with dependent variable p because C is a function of Re; Re in turn depends on p.

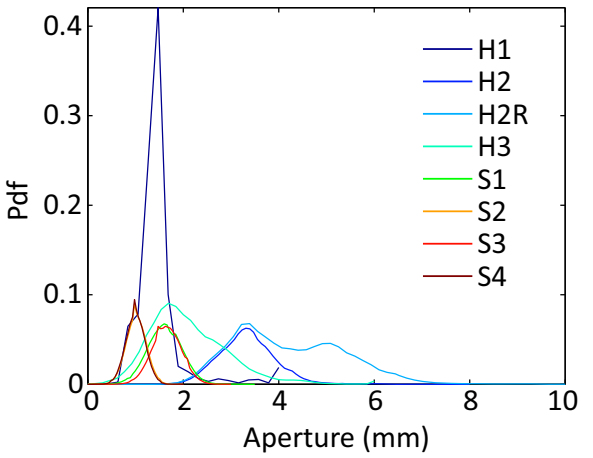

Figure 5. Probability density function of aperture fields for natural fractures mapped with HRXCT denoted by labels beginning with "H" and synthetic fractures generated with the program SynFrac [*Ogilvie et al*., 2006] denoted by labels beginning with "S." One of the natural fractures (H2) was artificially roughened to generate fracture H2R.

3. Methodology

3.1. Real and Synthetic Three-Dimensional Fractures

Three natural welded Santana tuff samples collected from Closed Canyon, Big Bend National Park, Texas, USA, were scanned at the high-resolution X-ray computed tomography (HRXCT) facility at The University of Texas at Austin. The approach used here was described in detail by *Ketcham et al*. [2010] and *Slottke* [2010]. The size and horizontal resolution of the scanned fractures, labeled with an initial "H," and its statistical properties are shown in Table 1. The vertical resolution for the natural fractures was set at ~0.25 mm.

To further test the validity of the MLCL for various types of fractures, we generated four self-affine fractures through the program SynFrac with the same parameters described by *Ogilvie et al*. [2006]. Here we used a different resolution/grid spacing to make it more similar to the scanned real fractures. We generated synthetic fractures with 512 × 512 points per fracture surface, regardless of fracture size, although the sizes were also similar to the scanned fractures. Further, we assigned a minimum $b = 10$ μm whenever aperture is zero in order to maintain mesh quality and due to difficulties in mesh generation. Therefore, the statistical properties of the synthetic fractures varied slightly from those in *Ogilvie et al*. [2006] (Table 1). The synthetic fractures are denoted with an initial "S." In order to specifically test for local roughness effects, one of the natural fractures (H2) was further roughened by increasing the local aperture gradient by 1.5 times; this fracture is now denoted as H2R.

The synthetic fractures used here, to some extent, have been shown to represent the hydraulic properties of fractures within igneous, sedimentary, and metamorphic rocks [*Ogilvie et al*., 2006]. The probability density function of the b fields for the natural and synthetic fractures is shown in Figure 5. In general, aperture fields for S1–S4 and H2 roughly follow a Gaussian distribution, while aperture fields for H1 and H3 roughly follow a non-Gaussian distribution skewed toward smaller and larger values, respectively. Moreover, the artificially generated aperture field H2R created by increasing local aperture gradient shows a bimodal distribution; this property may probably lead to the difficulty of predicting flow rate by simply using the LCL. The arithmetic means of b range from 1.00 to 4.22 mm and the standard deviations of b range from 0.20 to 1.18 mm. Although the fracture dimensions are identical, the natural fracture apertures are relatively more heterogeneous compared to the synthetic fractures (Table 1).

3.2. Direct Numerical Simulations of Flow Fields

The numerical experiments used computational fluid dynamics (CFD) simulations for flow through 3-D fractures. The CFD modeling, where the NSE with gravitational effects ignored was directly solved, was implemented through the generic finite element software COMSOL Multiphysics. We assigned fracture surfaces (without a skin or rind) and sides as no-slip boundaries on the premise of no interaction with the matrix, and applied a pressure drop $\Delta p = 0.01$ Pa over the fracture length. Standard fluid properties for water were prescribed: $\rho = 1000$ kg/m^3 and $\mu = 1 \times 10^{-3}$ Pa s. The fractures were discretized into ~10 million tetrahedral elements with smaller elements (~0.2 mm) along the boundaries (Figure 6). Numerical experiments were conducted in a high-performance workstation, with each steady state solution taking as much as 2 days to converge. For each fracture case, we conducted a pair of simulations where flow was either in the x or y direction. Sensitivity analysis showed negligible numerical dispersion for the given mesh discretization schemes.

3.3. Implementation of Modified Local Cubic Law

We solved equation (12) numerically through COMSOL Multiphysics. The equation was solved iteratively because of its nonlinear nature. The correction with C was implemented via interpolation. That is, at each

iteration, in the numerical solution of (12), C was calculated and linearly interpolated, and extrapolated as a constant value when necessary, based on the discrete data. Re was updated using C during each iteration.

The inlet/outlet boundary conditions were the same as those used for the direct 3-D CFD simulations, but here we assigned no-flux boundaries for the edges. The rectangle mesh size was specified so that the original fracture resolution was retained and trivial numerical dispersion occurred. Unlike the direct CFD simulations, which sometimes took days to converge, the numerical simulations with equation (12) took a few minutes.

3.4. Assessment of the Accuracy of the Modified Local Cubic Law

The potential advantage and advancement of the MLCL in prediction of local velocities and volumetric flow rate are the combination of all corrective aspects that have been considered and studied separately [*Brown*, 1987; *Zimmerman et al*., 1991; *Mourzenko et al*., 1995; *Ge*, 1997; *Brush and Thomson*, 2003; *Al-Yaarubi et al*., 2005], including local tortuosity, roughness, and low inertial force.

The overall performance of the MLCL is evaluated via quantifying the effective errors in predicting volumetric flow rates as δ:

$$\delta_i = \frac{Q_i - Q_{\mathrm{NSE}}}{Q_{\mathrm{NSE}}} \times 100\% \tag{13}$$

where Q_{NSE} is volumetric flow rate at the outlet boundary calculated in the 3-D CFD simulations (Q_{NSE} is considered as the "true" volumetric flow rate), Q_i is volumetric flow rate at the outlet boundary calculated through equations (3), (6), (12), and (15) (see below), where i = equation number.

An alternative way to assess the performance of the MLCL is to break down the effective errors into local errors $\xi_i(x, y)$ in terms of volumetric flow rate, which is described mathematically by:

$$\xi_i(x,\ y) = \frac{Q_i(x,\ y) - Q_{\mathrm{NSE}}(x,\ y)}{Q_{\mathrm{NSE}}(x,\ y)} \times 100\% \tag{14}$$

where $Q_{\mathrm{NSE}}(x, y)$ is the local vertically integrated volumetric flow rate calculated from CFD simulation results, and $Q_i(x, y)$ is the local volumetric flow rate calculated from equations (3) and (12), where i refers to equation number or model type, i.e., LCL and MLCL, respectively.

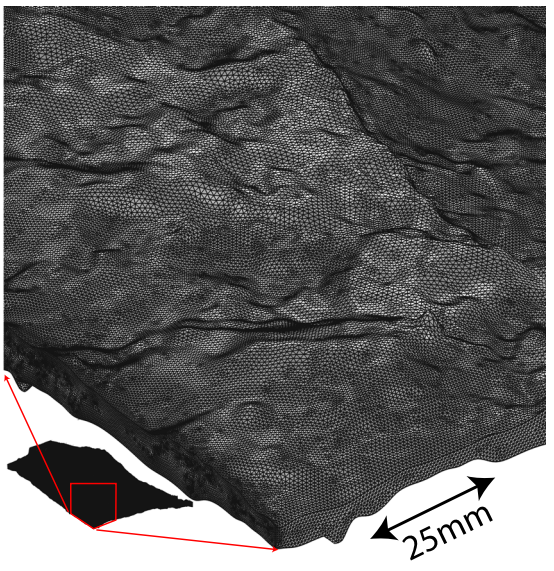

Figure 6. Illustration of the tetrahedral mesh used in the finite element model of fracture H3. The inset red polygon shows the portion of the fracture that is illustrated. There are ~10 million tetrahedral elements, with 7.2×10^5 triangular boundary elements and 4144 edge elements. Element size is about 0.2 mm.

3.5. Comparison of the Modified Local Cubic Law With Other Models

To highlight the strength of the MLCL, we conducted numerical simulations using the governing equation from *Ge* [1997] through the finite element method also implemented in COMSOL Multiphysics, and using the modified LCL as formulated by *Brush and Thomson* [2003] through a finite-volume approach we implemented in MATLAB. In the latter, grid blocks serve as control volume with the modified harmonic average aperture representing the transmissivity at the face of the control volume. The effective errors associated with *Ge*'s derivation and *Brush and Thomson*'s formulation are denoted as δ_{Ge} and δ_{Brush}, respectively; they are quantified through equation (13), where Q_i is replaced by volumetric flow rate from the corresponding numerical simulations at the outlet boundary. We also evaluate $\xi_i(x, y)$ in the x direction following (14) with calculations using *Ge*'s [1997] derivation and *Brush and Thomson*'s [2003] approach.

The Cubic Law (CL) when also scaled by a factor that corrects for the discrepancy between hydraulic and geometric apertures can give volumetric flow rates similar to those based on the LCL [*Renshaw*, 1995]. Thus, we additionally assess the accuracy of the CL in predicting volumetric flow rate following the approximation recommended by *Renshaw* [1995], where the modified aperture field accounting for the local tortuosity and roughness is used, which is described by:

$$Q = \frac{\rho g < b_{fR} >^3}{12\mu} WI \left[1 + \left(\frac{\sigma_{b_{fR}}}{< b_{fR} >}\right)^2\right]^{-1.5} \tag{15}$$

where b_{fR} is the modified aperture field with arithmetic mean $< b_{fR} >$ and standard deviation σ_{bfR}, g is the gravitational acceleration, W is the fracture width, and I is the hydraulic gradient. In this case, we neglect inertial force since we do not have prior knowledge of the Re field to correctly use C. However, for tortuosity/roughness-dominated regimes where the inertial effect is relatively negligible ($Re < 1$), $C(R1, R2, Re)$ can be reduced into $C_R(R1, R2)$. Therefore, the b field can be transformed into a tensor field with x and y principal components allowing for consideration of the effects of the local tortuosity and roughness following equation (12), which is:

$$b_{fR} = \begin{bmatrix} \left(\frac{12\mu T_x \cos(\varnothing_x)}{C_R}\right)^{1/3}, & 0 \\ 0, & \left(\frac{12\mu T_y \cos(\varnothing_y)}{C_R}\right)^{1/3} \end{bmatrix} \tag{16}$$

4. Results

4.1. Failure of the Local Cubic Law

The validity of the LCL (equation (3)) was tested through comparison between volumetric flow rates from solving the LCL and from solving the NSE with CFD simulations. The simulated flow fields for the studied fractures are exemplified in Figure 7. The natural fractures clearly demonstrate preferential or channeling flow following the most conductive region, whereas the synthetic fractures show more dispersed flow paths without apparent preferential flow. The artificially roughened natural fracture (H2R) produced slow flowing or stagnation and/or recirculation zones as illustrated by the broader areas with blue colors (Figure 7; blue corresponds to smaller velocities) near the fracture walls.

The LCL is widely known to overestimate flow rate through fractures even at low Re (<1) regimes [*Nicholl et al*., 1999]; our results further confirm this (Figure 8). The effective errors (δ_3) in using the LCL range from 22.0% to 70.7% (Table 2), with the magnitude depending on the geometric properties of fractures, i.e., roughness and tortuosity. Even worse, the local error (ξ_{LCL}) in volumetric flow rate defined in equation (14) may increase up to 200% (Figures 9 and 10a). Not only do our results agree with previous studies showing overestimation of bulk flow rates [*Zimmerman and Yeo*, 2000; *Zimmerman et al*., 2004], the results also highlight the overestimation in local flow rates, with only a minority of ξ_{LCL} below 0 (Figure 10a). The results show, however, that underestimation of local flow rate is possible via solving the MLCL. This can be caused by inherent deficiencies with correcting through C to reproduce more complex local nonparabolic velocity profiles at wedge boundaries associated with local roughness.

Natural fractures have prominent areas of high ξ_{LCL} showing long-range correlation effect, whereas the synthetic fractures show a more dispersed pattern of ξ_{LCL} with random distribution (Figure 9). The probability density functions of ξ_{LCL} for all studied fractures show a fairly normal distribution, with median values greater than 0 that varies from fracture to fracture (Figure 10a). The patterns in ξ_{LCL} integrate contributions from aperture, tortuosity, and roughness. To potentially identify individual contributions, we plot ξ_{LCL} as defined by equation (14) against aperture (Figure 11), tortuosity τ (Figure 12), and aperture gradient $R1$ (Figure 13).

ξ_{LCL}, somewhat surprisingly, generally increases with aperture, with a slight exception for H1 (Figure 11), but has no clear trend with τ and $R1$ (Figures 12 and 13). This shows that the aperture values may dominate over τ and $R1$ in determining ξ_{LCL} for our studied fractures. The signal of ξ_{LCL} induced by τ and $R1$ might be

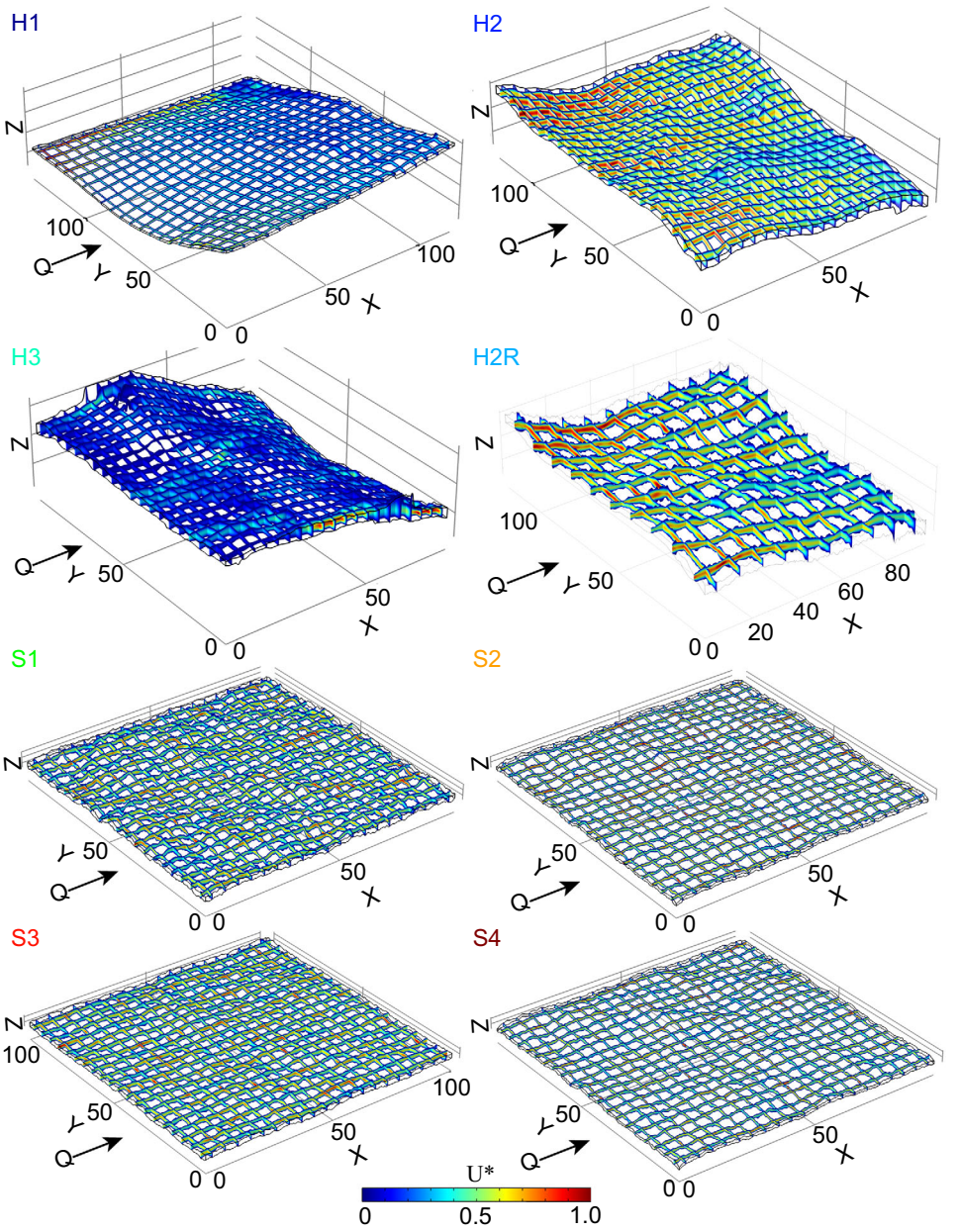

Figure 7. Three-dimensional fracture velocity fields (U*, denoted by the color) from CFD simulations. U* is defined as $U^* = U/U_{max}$, where U is the velocity magnitude and U_{max} is the maximum velocity magnitude. The fractures correspond to the fractures in Figure 5.

smeared out by aperture, such that they barely reach a systematic trend in the dependence of ξ_{LCL} on τ and $R1$ (Figures 12 and 13).

4.2. Accuracy and Validity of the Modified Local Cubic Law

The MLCL (equation (12)) is first verified using reliable CFD simulations of flow through natural and synthetic fractures in terms of predicting bulk volumetric flow rate. For Q_{12} derived from the MLCL, δ_{12} ranges from -3.3% to 13.4% with arithmetic mean $<|\delta_{12}|> = 3.7\%$ (Figure 8 and Table 2). Despite the different types of fractured rocks representing a range in spatial heterogeneity, effective volumetric flow rates predicted from the MLCL agree quite well with that from CFD simulations.

Not accounting for tortuosity contributes the most effective error relative to contributions from local roughness and inertia for most of the studied fractures with relatively smooth surfaces (Figure 8 and Tables 1 and

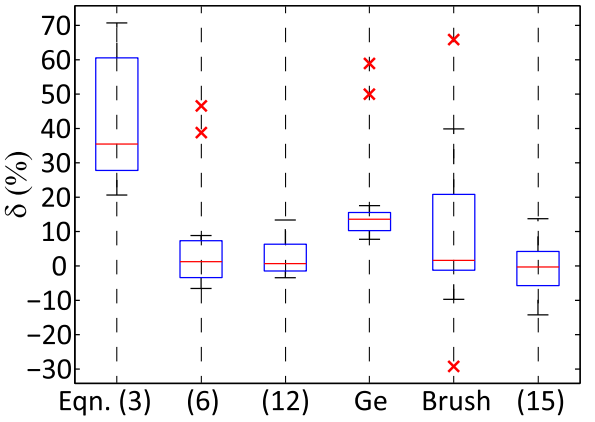

Figure 8. Statistics of effective errors (δ) shown by Box-Whisker plots. The effective errors are between "true" volumetric flow rates taken from CFD simulations and different versions of the LCL and CL, i.e., equations (3), (6), (12), and (15), *Ge*'s [1997] derivation and *Brush and Thomson*'s [2003] formulation. Negative values of δ indicate underestimation of flow rate; positive values correspond to overestimation. For quartiles, central mark (red line) refers to the median (50%), and the edges of the box are the 25th and 75th percentiles, respectively. The whiskers extend to the minimum and maximum data that are included in statistical analysis, while the extreme data are excluded (red crosses).

2). On the contrary, for roughened fracture H2R, effective error arising from the LCL will be significantly reduced by correction with C rather than solely correcting for tortuosity. In general, the classical LCL overestimates volumetric flow rate with δ_3 ranging from 22.0% to 70.7% with $<|\delta_3|> = 40.8\%$ (Table 2) depending on the degree of tortuosity and roughness. After accounting for tortuosity through equation (6), δ_6 decreases substantially with $<|\delta_6|> = 9.3\%$. Accounting for the local roughness and inertial effects via the MLCL further improves the performance of the LCL with $<|\delta_{12}|>$ decreasing to 3.7%.

To further test the validity of the MLCL, we compared predicted volumetric flow rates to experimentally measured flow rates for a rough-walled fracture mapped in high resolution, which was described and studied by *Cardenas et al*. [2007]. The flow experiments were described by *Slottke* [2010]. The experiments ranged from Darcy to Forchheimer flows with varying imposed head gradients [*Slottke*, 2010]. We selected three cases with increasing *Re* where Darcy flow still holds. The evaluation of δ_{12} was done by replacing Q_{NSE} in equation (13) with volumetric flow rates from the experimental flow tests. The resultant δ_{12} is 2.3%, 6.0%, and 9.1% which reveals the robustness of the MLCL for predicting actual flow rates.

Moreover, the MLCL reduces local errors by improving the prediction of local flow rate. Using the classical LCL, the probability density function of ξ_{LCL} follows a normal distribution with a large standard deviation and median value greater than 0. Using the MLCL, the standard deviation in ξ_{MLCL} is reduced and the median value becomes close to 0 (Figure 10). However, the broad relationships between ξ and fracture geometric (Figures 11–13) are similar for both the LCL and MLCL. That is, the contribution to ξ_{MLCL} from aperture is systematic compared to that from tortuosity and roughness; the same patterns were observed for ξ_{LCL}. Figure 12 also shows that, to some extent, the MLCL is likely to underestimate local flow rate when $1/\tau < 0.6$. τ is tortuosity as defined in Figure 1.

Table 2. Effective Errors in Volumetric Flow Rate (δ) Predicted Using Different Versions of the LCL and CL, i.e., Equations (3), (6), (12), and (15), *Ge*'s [1997] Derivation and *Brush and Thomson*'s [2003] Formulation Compared to that Calculated Through CFD Simulations[a]

Fracture	Direction	δ_3 (%)	δ_6 (%)	δ_{12} (%)	δ_{15} (%)	δ_{Ge} (%)	δ_{Brush} (%)
H1	*x*	22.03	8.00	7.08	13.76	14.10	−9.71
	y	26.70	−0.61	0.33	−14.24	9.15	22.99
H2	*x*	24.39	6.71	5.87	11.24	8.17	−1.41
	y	20.64	8.84	7.93	9.69	11.38	18.69
H3	*x*	57.87	−4.03	−2.36	2.23	7.76	39.86
	y	32.00	4.34	2.93	5.79	14.67	−29.18
S1	*x*	63.19	−4.35	−1.89	−5.38	17.55	−1.10
	y	63.99	−6.55	−3.44	−8.55	16.41	−2.24
S2	*x*	37.53	−2.41	−0.34	−6.06	13.10	2.29
	y	37.90	−5.58	−3.26	−8.71	11.56	−0.31
S3	*x*	28.87	−1.92	−0.59	−3.13	10.38	0.93
	y	29.16	−2.75	−1.03	−2.88	10.15	0.73
S4	*x*	35.54	3.51	1.56	0.37	14.58	5.64
	y	35.43	3.08	1.01	−0.96	14.47	6.03
H2R	*x*	66.49	38.91	6.81	1.57	50.10	34.38
	y	70.71	46.69	13.38	2.62	59.03	65.86

[a]The statistics of effective errors can be found in Figure 8.

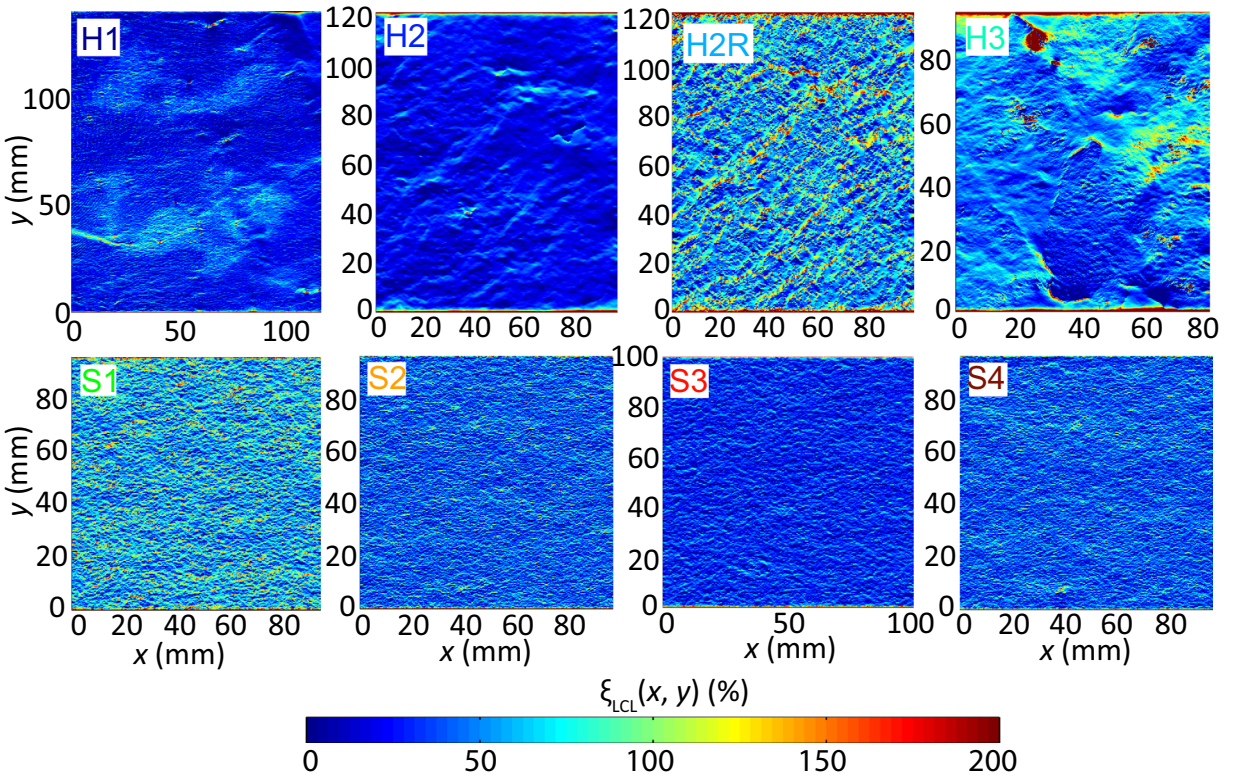

Figure 9. Spatial distribution of local error (ξ_{LCL}) in local volumetric flow rate by using the classical Local Cubic Law (LCL). $\xi(x, y)$ is defined in equation (14). The fractures correspond to the fractures in Figure 5.

5. Discussion

5.1. Performance of the Modified Local Cubic Law Relative to Other Models

The MLCL performs better than *Ge*'s and *Brush and Thomson*'s approaches (Figure 8 and Table 2). For the studied fractures, $<|\delta_{Ge}|>$ is 17.7% and $<|\delta_{Brush}|>$ is 15.5%; both methods are less accurate than $<|\delta_{12}|>$ (Table 2). Moreover, the standard deviation of $|\delta_{Brush}|$, denoted as $\sigma_{|\delta Brush|}$, is 18.9%, followed by $\sigma_{|\delta Ge|} = 14.8\%$ for *Ge*'s derivation, and the MLCL has the lowest $\sigma_{|\delta 12|} = 3.6\%$ (Figure 8).

We also analyzed how δ changes with increasing combined aperture deviation and tortuosity for different versions of the LCL (Figure 14). For relatively smooth fractures, $|\delta_{MLCL}|$ (i.e., $|\delta_{12}|$) and $|\delta_{Ge}|$ roughly follow the same trend for the studied fractures with values fluctuating about their mean, but $|\delta_{MLCL}|$ is always less than $|\delta_{Ge}|$ because of the MLCL's improvements over *Ge*'s governing equation by allowing for local roughness and inertial effects. Moreover, a previous study confirmed that *Ge*'s theory is more appropriate for tortuous than rougher fractures [*Nicholl et al*., 1999]. Our results further show the shortcomings and applicability of *Ge*'s theory. It fairs poorly when applied to the roughened fracture H2R, but performs relatively well for the more tortuous fracture H3 (Figure 14 and Table 2). Figure 10c illustrates the performance of *Ge*'s derivation when applied to a rougher fracture; the median of ξ_{Ge} for H2R deviates further away from 0. The MLCL corrects for this shortcoming by considering for the convergence and divergence in the aperture field.

For relatively smooth fractures, flow modeling with the finite-volume method with effective transmissivity based on *Brush and Thomson* [2003] predicts volumetric flow rates better than the MLCL (Figure 14); that is $|\delta_{Brush}| < |\delta_{MLCL}|$. However, $|\delta_{Brush}|$ increases for rougher and more tortuous fractures, while $|\delta_{MLCL}|$ remains $<10\%$. Similar to the effective error, the local error ξ_{Brush} follows a normal distribution with median value close to 0 for relative smooth fractures. But the median of ξ_{Brush} deviates from 0 for the more tortuous fracture (H3) and the roughened fracture (H2R) (Table 2 and Figure 10d). Yet, the MLCL's accuracy for such cases still holds.

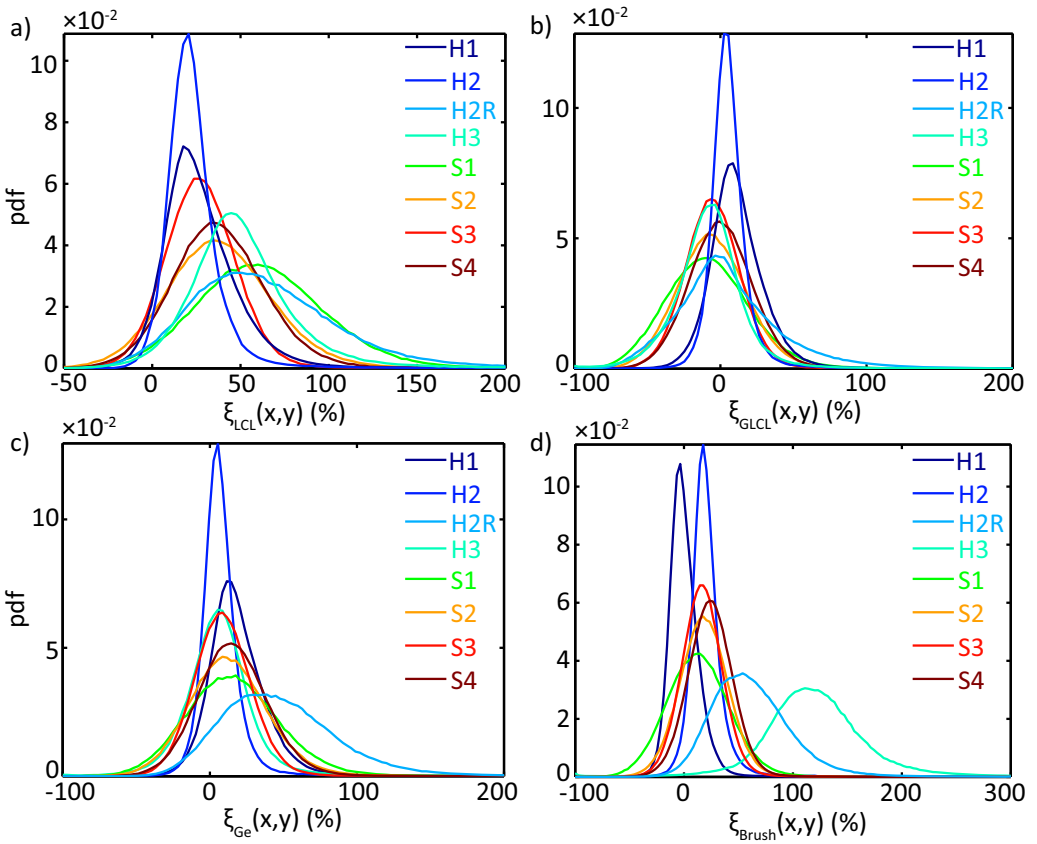

Figure 10. Probability density function of errors ($\xi(x, y)$) in local volumetric flow rate by using (a) Local Cubic Law (LCL), (b) modified Local Cubic Law (MLCL), (c) *Ge*'s [1997] method, and (d) *Brush and Thomson*'s [2003] formulation. The fractures correspond to the fractures in Figure 5.

The MLCL is shown to be an accurate predictor for effective volumetric flow rate, but the fluctuation in $|\delta_{\mathrm{MLCL}}|$ is counterintuitive since we expect that $|\delta_{\mathrm{MLCL}}|$ would increase with global roughness and tortuosity. One possible reason could be attributed to the construction of C; it only considers zero-velocity in the z direction on the wedge boundary with specified constant pressure, while this is not the case for the rough

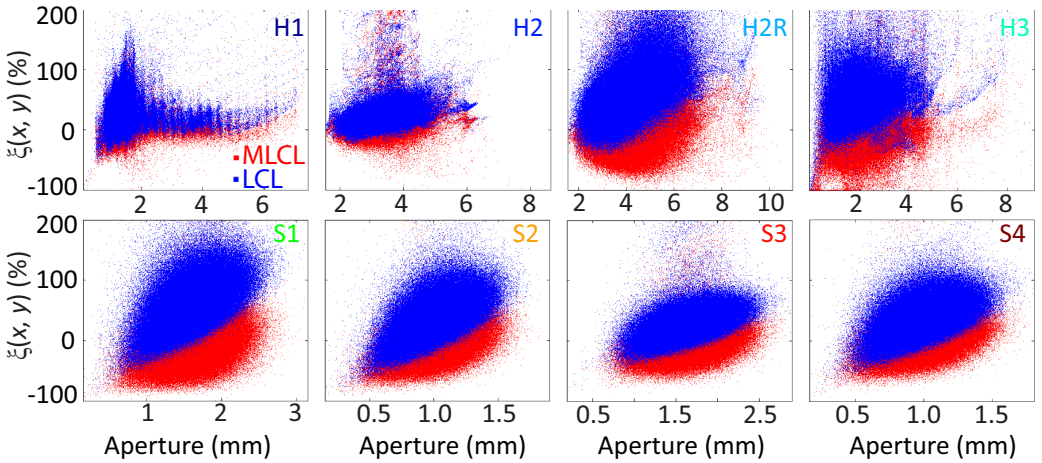

Figure 11. Dependence of errors ($\xi(x, y)$) in local volumetric flow rate on aperture. Blue filled squares represent solutions from solving the Local Cubic Law (LCL), while the red filled squares from solving the modified LCL (MLCL). The fractures correspond to the fractures in Figure 5.

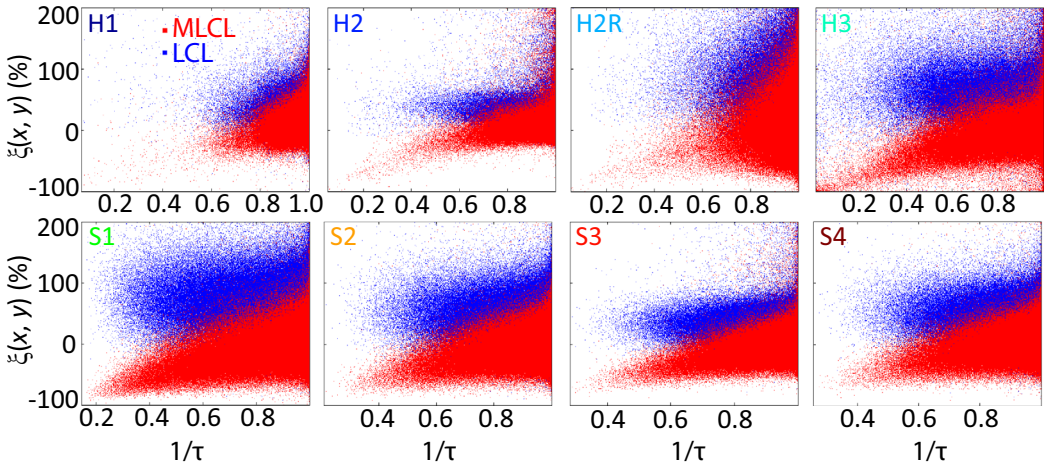

Figure 12. Relationship between errors ($\xi(x, y)$) in local volumetric flow rate and tortuosity (τ). Blue filled squares represent solutions from solving the Local Cubic Law (LCL), while the red filled squares from solving the modified LCL (MLCL). The fractures correspond to the fractures in Figure 5.

fracture, which might lead to different behavior in C. Although the method of developing C is not perfect, the overall MLCL's performance is quite good (Table 2). Future studies could explore C which allows for non-parabolic velocity profiles on the boundary in order to further improve the MLCL.

5.2. Application of the Modification to the Cubic Law

Overall, the CL with modified aperture performs well in terms of matching the volumetric flow rate from CFD simulations at laminar regimes. Effective errors in flow rate δ_{15} range more broadly from −14.2% to 13.8%, with just a slightly higher mean of 6.1% relative to that resulting from the MLCL (Figure 8 and Table 2). Though, unlike other previous modified versions of the LCL, the modified CL is sufficient to estimate an effective flow rate for rougher fracture H2R. Using the CL method without taking into account local tortuosity and roughness would result in effective errors (δ) ranging from −78.0% to −8.8%, with arithmetic mean and standard deviation of absolute value ($|\delta|$) equal to 40.4% and 18.6%, respectively (results are not shown here). Clearly, the CL when implemented with the modified aperture field is greatly improved and could be an accurate predictor for the hydraulic properties of single fractures that are tortuosity/roughness dominated. That is, the predicted hydraulic properties, and by consequence the predicted volumetric flow rates, would be similar to those calculated via direct numerical simulations.

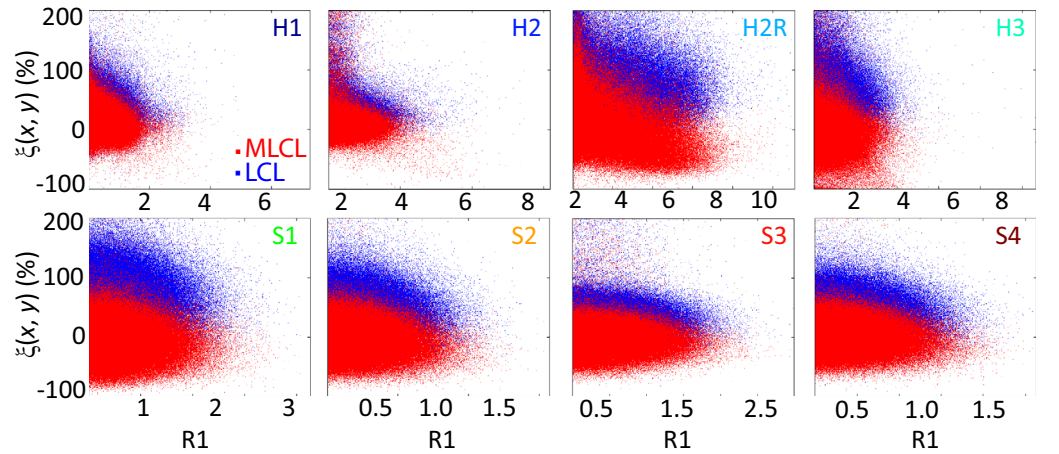

Figure 13. Relationship between errors ($\xi(x, y)$) in local volumetric flow rate and $R1$ defined in equation (7). Blue filled squares represent solutions from solving the Local Cubic Law (LCL), while the red filled squares from solving the modified LCL (MLCL). The fractures correspond to the fractures in Figure 5.

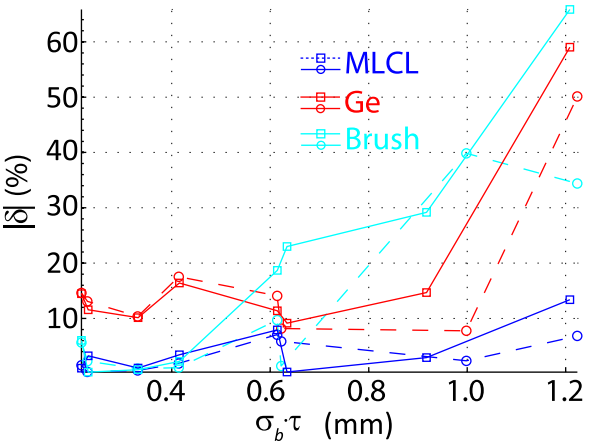

Figure 14. Effective errors (δ) for different natural and synthetic fractures plotted for varying products of aperture deviation (σ_b) and effective tortuosity (τ). The error is defined in equation (13) between "true" volumetric flow rates taken from CFD simulations and different versions of the Local Cubic Law, i.e., modified LCL (MLCL) developed in this study, *Ge*'s [1997] deviation, and *Brush and Thomson*'s [2003] formulation. τ is the ratio of the tortuous area of the fracture midsurface to its projected area in the *x*-*y* plane. *b* is the apparent aperture with standard deviation (σ_b). Dashed lines with circles correspond to flow rates in the *x* direction, while solid lines with squares are for the *y* direction.

5.3. Limitation of the Modified Local Cubic Law

Although the MLCL improves the performance of the classical LCL, there are still a few assumptions undermining its performance in terms of completely replacing the NSE. After all, a 2-D vertically-integrated version of NSE cannot fully represent the 3-D NSE. The key limitation of the MLCL rests on, as mentioned previously, the determination of *C*. Recall that *C* was estimated based on fluid flow through simple 2-D symmetric wedges with constant pressure boundary conditions, and thus perfectly parabolic velocity profiles. However, flow through local 3-D asymmetric wedges with nonparabolic velocity boundary conditions is expected to occur. Moreover, eddies may occupy several neighboring 3-D wedges; eddies are constrained to the 2-D wedges in our case. Additionally, inertial force is not fully considered in this study in order to generate a more comprehensive form for *C* (here local $Re \leq 1$ only). Laminar flow through 3-D rough-walled fractures may lead to local $Re > 1$ and our current version for *C* does not account for this. These aspects should be explored in the future by using the same approach presented here.

Furthermore, the MLCL is based on the premise of absence of the off-diagonal terms in the tensorial hydraulically equivalent aperture (equation (16)) and transmissivity (equation (12)). That is, we assume the global coordinate is aligned with the local principal axes, even though this assumption may be violated. Future studies should thus focus on generating *C* using 3-D wedges with the application of various boundary conditions to further improve the MLCL. This will allow for the simultaneous consideration of the full transmissivity tensor with local principal axes uniquely depending on the local midsurface of fractures [*Mallikamas and Rajaram*, 2010]. In spite of those intrinsic shortcomings, the current version of the MLCL performs well in terms of predicting effective and local flow rates, and provides a viable method for further consideration of a broad range of *Re* and realistic nonparabolic velocity profiles within and on the boundary of 3-D wedges.

6. Summary and Conclusions

The Local Cubic Law (LCL) (equation (3)) is a widely applied model for predicting fluid flow field in fractures. However, there are still unresolved issues in the application of the LCL including errors due to local tortuosity, roughness, and inertial effects. We present the modified Local Cubic Law (MLCL) (equation (12)) that corrects the LCL for the sources of error. To test the validity of the MLCL with direct simulations and physical experiments, we used maps of natural fractures, synthetic fractures generated by the program SynFrac, and one artificially roughened fracture produced by increasing the local aperture gradient of one of the natural fracture maps.

Overall, the MLCL performs better than previous versions of the LCL regardless of fracture local tortuosity and roughness. For the studied fractures, the effective errors (δ) (equation (13)) of the MLCL range from -3.4% to 13.4 with arithmetic mean of $|\delta|$ ($<|\delta|>$) equal to 3.7%. While $<|\delta|>$ are 40.8% for the traditional LCL, 17.7% for *Ge*'s model, and 15.1% for *Brush and Thomson*'s formulation (Figure 8). Importantly, for more tortuous and rougher fractures, the modified version of the LCL proposed by *Brush and Thomson* [2003] leads to considerable errors in predicting effective and local volumetric flow rates (Figures 8 and 10 and

Table 2). Furthermore, *Ge*'s model performs relatively well for tortuous fractures, but its performance worsens for rougher fractures (Table 2). However, using the Cubic Law with a modified aperture field will improve the prediction of effective volumetric flow rate with only a slightly higher $<|\delta|> = 6.1\%$ than the MLCL. Importantly, the application of the MLCL to the modified CL allows for predicting the fracture hydraulic properties based on the geometric information within a low range of local *Re* (≤ 1).

The MLCL developed here provides an approach for accurately calculating the hydraulic properties and local vertically integrated flow fields for rough and tortuous fractures; it may thus be suitable for integration with and improvement of fracture network models. The MLCL would also provide more accurate flow fields for solute and heat transport problems. Since we used relatively smooth fractures with only one artificially roughened fracture in this study, testing the performance of the MLCL by using rougher fractures should be a goal for future work.

Acknowledgments

Data set of *C*(*R*1, *R*2, *Re*) supporting equation (12) is provided in the supporting information data set S01. This work was supported as part of the Center for Frontiers of Subsurface Energy Security (CFSES) at the University of Texas at Austin, an Energy Frontier Research Center funded by the U.S. Department of Energy, Office of Science, Office of Basic Energy Sciences under award DE-SC0001114. Additional support was provided by the Geology Foundation of the University of Texas. The imaging of the fractures was supported by the National Science Foundation (EAR-0439806 grant to J.M. Sharp and R.A. Ketcham, and EAR-0345710 to Ketcham). We thank Editor Harihar Rajaram, Associate Editor Russell Detwiler, reviewers Robert Zimmerman, Carl E. *Renshaw*, In Wook Yeo, and two anonymous reviewers for their constructive comments in evaluating this manuscript.

References

Al-Yaarubi, A. H., C. C. Pain, C. A. Grattoni, and R. W. Zimmerman (2005), Navier-Stokes simulations of fluid flow through a rough fracture, in *Dynamics of Fluids and Transport in Fractured Rock, Geophys. Monogr. Ser.*, vol. 162, edited by B. Faybishenko, P. A. Witherspoon, and J. Gale, pp. 55–64, AGU, Washington, D. C.

Basha, H. A., and W. El-Asmar (2003), The fracture flow equation and its perturbation solution, *Water Resour. Res.*, *39*(12), 1365, doi:10.1029/2003WR002472.

Brown, S. R. (1987), Fluid flow through rock joints: The effect of surface roughness, *J. Geophys. Res.*, *92*(B2), 1337–1347, doi:10.1029/JB092iB02p01337.

Brown, S. R., H. W. Stockman, and S. J. Reeves (1995), Applicability of the Reynolds equation for modeling fluid flow between rough surfaces, *Geophys. Res. Lett.*, *22*(18), 2537–2540, doi:10.1029/95GL02666.

Brush, D. J., and N. R. Thomson (2003), Fluid flow in synthetic rough-walled fractures: Navier-Stokes, Stokes, and local cubic law simulations, *Water Resour. Res.*, *39*(4), 1085, doi:10.1029/2002WR001346.

Cardenas, M. B., D. T. Slottke, R. A. Ketcham, and J. M. Sharp Jr. (2007), Navier-Stokes flow and transport simulations using real fractures shows heavy tailing due to eddies, *Geophys. Res. Lett.*, *34*, L14404, doi:10.1029/2007GL030545.

Cardenas, M. B., D. T. Slottke, R. A. Ketcham, and J. M. Sharp Jr. (2009), Effects of inertia and directionality on flow and transport in a rough asymmetric fracture, *J. Geophys. Res.*, *114*, B06204, doi:10.1029/2009JB006336.

Chaudhary, K., M. B. Cardenas, W. Deng, and P. C. Bennett (2011), The role of eddies inside pores in the transition from Darcy to Forchheimer flows, *Geophys. Res. Lett.*, *38*, L24405, doi:10.1029/2011GL050214.

Chaudhary, K., M. B. Cardenas, W. Deng, and P. C. Bennett (2013), Pore geometry effects on intrapore viscous to inertial flows and on effective hydraulic parameters, *Water Resour. Res.*, *49*, 1149–1162, doi:10.1002/wrcr.20099.

Detwiler, R. L., H. Rajaram, and R. J. Glass (2000), Solute transport in variable-aperture fractures: An investigation of the relative importance of Taylor dispersion and macrodispersion, *Water Resour. Res.*, *36*(7), 1611–1625, doi:10.1029/2000WR900036.

Detwiler, R. L., H. Rajaram, and R. J. Glass (2002), Experimental and simulated solute transport in a partially-saturated, variable-aperture fracture, *Geophys. Res. Lett.*, *29*(8), doi:10.1029/2001GL013508.

Elkhoury, J. E., P. Ameli, and R. L. Detwiler (2013), Dissolution and deformation in fractured carbonates caused by flow of CO_2-rich brine under reservoir conditions, *Int. J. Greenhouse Gas Control*, *16*, suppl. 1, S203–S215, doi:10.1016/j.ijggc.2013.02.023.

Ge, S. (1997), A governing equation for fluid flow in rough fractures, *Water Resour. Res.*, *33*(1), 53–61, doi:10.1029/96WR02588.

Ketcham, R. A., D. T. Slottke, and J. M. Sharp (2010), Three-dimensional measurement of fractures in heterogeneous materials using high-resolution X-ray computed tomography, *Geosphere*, *6*(5), 499–514, doi:10.1130/ges00552.1.

Konzuk, J. S., and B. H. Kueper (2004), Evaluation of cubic law based models describing single-phase flow through a rough-walled fracture, *Water Resour. Res.*, *40*, W02402, doi:10.1029/2003WR002356.

Lee, S. H., K.-K. Lee, and I. W. Yeo (2014), Assessment of the validity of Stokes and Reynolds equations for fluid flow through a rough-walled fracture with flow imaging, *Geophys. Res. Lett.*, *41*, 4578–4585, doi:10.1002/2014GL060481.

Mallikamas, W., and H. Rajaram (2010), An improved two-dimensional depth-integrated flow equation for rough-walled fractures, *Water Resour. Res.*, *46*, W08506, doi:10.1029/2009WR008779.

Mourzenko, V., J.-F. Thovert, and P. Adler (1995), Permeability of a single fracture: Validity of the Reynolds equation, *J. Phys. II*, *5*(3), 465–482, doi:10.1051/jp2:1995133.

Nicholl, M. J., and R. L. Detwiler (2001), Simulation of flow and transport in a single fracture: Macroscopic effects of underestimating local head loss, *Geophys. Res. Lett.*, *28*(23), 4355–4358, doi:10.1029/2001GL013647.

Nicholl, M. J., H. Rajaram, R. J. Glass, and R. Detwiler (1999), Saturated flow in a single fracture: Evaluation of the Reynolds equation in measured aperture fields, *Water Resour. Res.*, *35*(11), 3361–3373, doi:10.1029/1999WR900241.

Ogilvie, S. R., E. Isakov, and P. W. J. Glover (2006), Fluid flow through rough fractures in rocks. II: A new matching model for rough rock fractures, *Earth Planet. Sci. Lett.*, *241*(3–4), 454–465, doi:10.1016/j.epsl.2005.11.041.

Renshaw, C. E. (1995), On the relationship between mechanical and hydraulic apertures in rough-walled fractures, *J. Geophys. Res.*, *100*(B12), 24,629–24,636, doi:10.1029/95JB02159.

Silliman, S. E. (1989), An interpretation of the difference between aperture estimates derived from hydraulic and tracer tests in a single fracture, *Water Resour. Res.*, *25*(10), 2275–2283, doi:10.1029/WR025i010p02275.

Sisavath, S., A. Al-Yaarubi, C. C. Pain, and R. W. Zimmerman (2003), A simple model for deviations from the Cubic Law for a fracture undergoing dilation or closure, *Pure Appl. Geophys.*, *160*(5), 1009–1022, doi:10.1007/PL00012558.

Slottke, D. T. (2010), Surface roughness of natural rock fractures: Implications for prediction of fluid flow, PhD dissertation, Univ. of Tex. at Austin, Austin.

Snow, D. T. (1969), Anisotropic permeability of fractured media, *Water Resour. Res.*, *5*(6), 1273–1289, doi:10.1029/WR005i006p01273.

Thompson, M. E., and S. R. Brown (1991), The effect of anisotropic surface roughness on flow and transport in fractures, *J. Geophys. Res.*, *96*(B13), 21,923–21,932, doi:10.1029/91JB02252.

Wang, L., and M. B. Cardenas (2014), Non-Fickian transport through two-dimensional rough fractures: Assessment and prediction, *Water Resour. Res.*, *50*, 871–884, doi:10.1002/2013WR014459.

Witherspoon, P. A., J. S. Y. Wang, K. Iwai, and J. E. Gale (1980), Validity of Cubic Law for fluid flow in a deformable rock fracture, *Water Resour. Res.*, *16*(6), 1016–1024, doi:10.1029/WR016i006p01016.

Zimmerman, R. W., S. Kumar, and G. S. Bodvarsson (1991), Lubrication theory analysis of the permeability of rough-walled fractures, *Int. J. Rock Mech. Min. Sci. Geomech. Abstr.*, *28*(4), 325–331, doi:10.1016/0148–9062(91)90597-f.

Zimmerman, R. W., D.-W. Chen, and N. G. W. Cook (1992), The effect of contact area on the permeability of fractures, *J. Hydrol.*, *139*(1–4), 79–96, doi:10.1016/0022–1694(92)90196-3.

Zimmerman, R. W., A. Al-Yaarubi, C. C. Pain, and C. A. Grattoni (2004), Non-linear regimes of fluid flow in rock fractures, *Int. J. Rock Mech. Min. Sci.*, *41*, suppl. 1, 163–169, doi:10.1016/j.ijrmms.2004.03.036.

Zimmerman, R. W., and I.-W. Yeo (2000), Fluid flow in rock fractures: From the Navier-Stokes equations to the Cubic Law, in *Dynamics of Fluids in Fractured Rock*, edited, 213–224 pp. American Geophysical Union, doi: 10.1029/GM122p0213.